Improvements in Saliency Tracking

For Use in Brushless DC Motors

by

Kai Yin

A Thesis Presented in Partial Fulfillment
of the Requirements for the Degree
Master of Science

Approved November 2021 by the
Graduate Supervisory Committee:

Sarma Vrudhula, Co-Chair
Shamala Chickamenahali, Co-Chair
Anamitra Pal

ARIZONA STATE UNIVERSITY

December 2021

ABSTRACT

Brushless DC (BLDC) motors are becoming increasingly common in various industrial and commercial applications such as micromobility and robotics due to their high torque density and efficiency. A BLDC Motor is a three-phase synchronous motor that is very similar to a non-salient Permanent Magnet Synchronous Motor (PMSM) with key differences lying in the non-ideal characteristics of the motor; the most prominent of these is BLDC motors have trapezoidal-shaped Back-Electromotive Force (BEMF). Despite their advantages, a present weakness of BLDC motors is the difficulty controlling these motors at standstill and low-speed conditions that require high torque. These operating conditions are common in the target applications and almost always necessitate the use of external sensors which introduce additional costs and points of failure. As such, sensorless based methods of position estimation would serve to improve system reliability, cost, and efficiency. High Frequency (HF) pulsating voltage injection in the direct axis is a popular method of sensorless control of salient-pole Interior-mount Permanent Magnet Synchronous Motors (IPMSM); however, existing methods are not sufficiently robust for use in BLDC and small Surface-mount Permanent Magnet Synchronous Motors (SPMSM) and are accompanied by other issues, such as acoustic noise. This thesis proposes novel improvements to the method of High Frequency Voltage Injection to allow for practical use in BLDC Motors and small SPMSM. Proposed improvements include 1) a hybrid frequency generator which allows for dynamic frequency scaling to improve tracking and eliminate acoustic noise, 2) robust error calculation that is stable despite the non-ideal characteristics of BLDC Motors, 3) gain engineering of Proportional-Integral (PI) type Phase-Locked-Loop (PLL) trackers that further lend stability, 4) observer decoupling mechanism to allow for seamless transition into state-of-the-art BEMF sensing methods at high speed,

and 5) saliency boosting that allows for continuous tracking of saliency under high torque load. Experimental tests with a quadrature encoder and torque efficiency calculations on a dynamometer verify the practicality of the proposed algorithm and improvements.

TABLE OF CONTENTS

Page

LIST OF TABLES v

LIST OF FIGURES vi

CHAPTER

1 INTRODUCTION 1

2 MODEL OF THE MOTOR 5

2.1 Mathematical Model of Synchronous Machines 5

2.2 Sources of Saliency 6

2.2.1 Reluctance Saliency 7

2.2.2 Saturation Saliency 7

3 METHOD OF HIGH FREQUENCY VOLTAGE INJECTION 9

3.1 Injection Voltage Generator 9

3.2 Injection Current Response and Extraction of Error Term 11

3.2.1 Error Calculation 12

3.3 Position Observer Construction 12

4 ISSUES WITH AND PROPOSED IMPROVEMENTS TO METHOD OF HIGH FREQUENCY VOLTAGE INJECTION FOR BLDC MOTORS 14

4.1 Issues and Proposed Improvements 14

4.2 Identification of Magnet Polarity 14

4.3 Acoustic Noise 18

4.3.1 Hybrid Frequency Injection 18

4.4 Variable Saliency 19

4.4.1 PLL Gain Engineering 19

CHAPTER Page

4.5 Integration with BEMF Methods 19
4.5.1 Observer Decoupling and Voltage Mixer 20
4.6 Loss of Saliency Signal 20
4.6.1 Adaptive Field Boost 21
4.7 Non-Ideal characteristics 21
5 OVERALL SYSTEM 22
6 EXPERIMENTAL RESULTS 24
6.1 Experimental Setup 24
6.2 Position Accuracy With Encoder 24
6.3 Encoder Results 26
6.4 Torque Efficiency 27
6.5 Torque Efficiency Results 29
7 CONCLUSION 32
REFERENCES 33
APPENDIX
A COLLECTED EXPERIMENTAL DATA 34

LIST OF TABLES

Table Page

1. Parameters of Motor Used in Encoder Test 24

2. Results of Encoder Test 26

3. Parameters of Motor Used in Torque Efficiency Test 28

4. Results of Torque Efficiency Test 30

LIST OF FIGURES

Figure Page

1. Rotor Flux Linkage as a Function of Stator Current 8
2. Diagram of Synchronous and Estimated Frames of Reference 11
3. Resultant D Axis Current When Polarity Is Correct 16
4. Resultant D Axis Current When Polarity Is Inverted 17
5. Overall System Diagram 22
6. Saliency Tracking Diagram 23
7. Image of Position Accuracy Experiment Setup 25
8. Results of Saliency Tracking Algorithm Compared to a Quadrature Encoder 26
9. Image of Motor Controller Hardware Used for Torque Efficiency 28
10. Results of Saliency Tracking Algorithm Compared to BEMF 29

Chapter 1

INTRODUCTION

Brushless DC and small Surface-Mount (i.e., Non-salient) Permanent Magnet Synchronous Motors (SPMSM) are seeing increasing use in industrial and commercial applications due to their high torque and power density, high efficiency, and wide operating region. A BLDC Motor is a three-phase synchronous motor that is very similar to a non-salient Permanent Magnet Synchronous Motor (PMSM) with key differences lying in the non-ideal characteristics of the motor; the most prominent of these is BLDC motors have trapezoidal-shaped Back-Electromotive Force (BEMF). Particular applications of interest for these motor types are micromobility and robotics. These applications are becoming increasingly popular due to other technological advancements making their usage more widely affordable and beneficial. Unlike other motor types, BLDC motors and PMSM require a sophisticated controller that must ascertain rotor position to properly control the motor. The most widely adopted control algorithm for the control of these motors is Field-Oriented Control (FOC). FOC is preferred over other control algorithms, such as Six-Step Block Commutation which is also known as Trapezoidal Control, because of its higher efficiency, improved dynamic response, and lower noise.

One downside of FOC is that it requires an accurate estimate of rotor position to properly control the motor. State-of-the-art FOC implementations typically employ sensorless methods to estimate rotor position as they do not introduce additional hardware and associated costs. A widely adopted method of sensorless position estimation in FOC is the measurement of Back-Electromotive Force or sensorless

BEMF. Sensorless BEMF works by estimating the BEMF induced by the rotation of rotor into the stator windings. There are several well-developed methods of accomplishing this [Zhang, Wang, and Xu 2017]. While existing sensorless BEMF methods are highly robust in the medium to high-speed region of operation, they either perform very poorly or do not function at all when the motor is at standstill or rotating at low speeds. There currently does not exist a robust state-of-the-art algorithm for the sensorless position estimation of BLDC motors and small non-salient PMSM at standstill or low speeds. As a result, there is a present weakness with these motors in low-speed high torque applications, such as mobility and robotics. Most systems that must overcome this weakness do so with the integration of sensors, such as hall sensors or quadrature encoders; however, these sensors incur additional costs, introduce additional points of failure, and do not provide the equivalent efficiency of sensorless methods. A sensorless method of rotor position estimation at standstill and low speeds would thus be extremely valuable for systems employing BLDC motors, especially those requiring high torque output at standstill or stating speed.

The Interior-Mount (i.e., Salient Pole) Permanent Magnet Synchronous Motor (IPMSM), a cousin of the BLDC and SPMSM, does not have this weakness in the standstill and low-speed region of operation. This is because saliency tracking methods of position estimation are able to ascertain rotor position by exploiting the extensive properties of the motor, namely rotor saliency. Rotor saliency is the position varying differential inductance of the stator windings. This results in a different inductance value for the motor's direct (D) axis and quadrature (Q) axis. Saliency tracking methods are robust with IPMSM because these motors feature rotor iron and are often specially designed to maximize rotor saliency. Unlike IPMSM, BLDC motors and SPMSM do not feature rotor iron, are designed without consideration to rotor saliency,

and thus have very weak and variable saliency. This causes existing saliency tracking methods to perform marginally at best. A popular method of saliency tracking is High Frequency (HF) Pulsating Voltage Injection [Wang, Valla, and Solsona 2020]. This method estimates position by injecting a voltage in the motor's estimated D axis and measuring the resulting current response to estimate the differential inductance. The differential inductance produces an error term in the position estimate which can be fed into a Phase-Locked Loop (PLL) to track rotor speed and position. This method is favored as it is relatively simple to integrate into existing FOC algorithms and is highly robust with IPMSM. It is worth noting that there are other saliency based methods of position estimation [Wang, Valla, and Solsona 2020] that can return a direct position estimate, but these are outside the scope of this thesis. As this thesis will discuss, there are a number of improvements that can be made with HF voltage injection to provide acceptable performance with BLDC motors. However, there are a number of issues that this method of saliency tracking must overcome in order to be viable in BLDC motors and SPMSM, namely these are: polarity resolution of magnet poles, variable and inconsistent saliency, reduction or elimination of acoustic noise, and integration with existing state-of-the-art BEMF methods for high-speed operation. This thesis presents improvements to the High Frequency (HF) Pulsating Voltage Injection method of saliency tracking that address the above issues for practical use in BLDC motors and small SPMSM. The proposed improvements include 1) a hybrid frequency generator which allows for dynamic frequency scaling to improve tracking and eliminate acoustic noise, 2) robust error calculation that is stable despite the non-ideal characteristics of BLDC Motors, 3) gain engineering of Proportional-Integral (PI) type Phase-Locked-Loop (PLL) trackers that further lend stability, 4) observer decoupling mechanism to allow for seamless transition into state-of-the-art BEMF

sensing methods at high speed, and 5) saliency boosting that allows for continuous tracking of saliency under high torque load.

Chapter 2

MODEL OF THE MOTOR

2.1 Mathematical Model of Synchronous Machines

The first matter to address is the difference between a BLDC motor and a PMSM. In essence, a BLDC motor is effectively an SPMSM with much greater non-ideal characteristics e.g., non-sinusoidal BEMF, stator reluctance, and can be modelled reasonably accurately as an SPMSM; BLDC motors do not contain rotor iron. Though non-ideal characteristics do impact performance, let us consider the PMSM model that ignores these, as this thesis will show they have negligible impact on the actual control of the motor. The synchronous voltages of the motor can be modelled from equation 2.1 [Liu et al. 2014]:

$$\begin{aligned} u_d &= r_s * i_d + L_d * \frac{di_d}{dt} - \omega_r * L_q * i_q \\ u_q &= r_s * i_q + L_q * \frac{di_q}{dt} - \omega_r * L_d * i_d + \omega_r * \Psi_f \end{aligned} \tag{2.1}$$

Where:

- u_q, u_q are the d and q axis voltages
- i_d, i_q are the d and q axis currents
- r_s is the line to neutral stator resistance
- Ψ_f is the permanent magnet flux linkage
- ω_r is the electrical speed of the rotor in radians per second

The synchronous axes are chosen such that the direct axis is the face of the north pole rotor magnet in a given pair of rotor magnets. The quadrature axis, as per

its name, leads the direct axis by 90°. This implies that the quadrature axis is the torque producing axis and also indicates direction of rotation. At standstill and low speed, the BEMF coupling terms ($\omega_r * \Psi_f$, $\omega_r * L_q * i_q$, $\omega_r * L_d * i_d$, are very small and tend to zero. At the frequencies of interest for HF voltage injection, the reactance will dominate the impedance, being at least an order of magnitude greater than the resistance. As a result, the equations can be simplified as follows [Liu et al. 2014]:

$$\begin{aligned} u_d &= L_d * \frac{di_d}{dt} \\ u_q &= L_q * \frac{di_q}{dt} \end{aligned} \tag{2.2}$$

From equation 2.2, we can see there are separate terms for the D axis inductance and Q axis inductance. Typically, these values are treated as equal during the analysis of SPMSMs, and in practice are often relatively similar in value, resulting in a small saliency ratio. Despite this, BLDC motors and SPMSM do feature some saliency, though the source of their saliency differs from that of IPMSM.

2.2 Sources of Saliency

Motor saliency is the differential inductance between a synchronous motor's direct axis and quadrature axis. There are two primary sources of saliency in synchronous motors featuring permanent magnet flux linkage: reluctance saliency and saturation saliency.

2.2.1 Reluctance Saliency

The primary source of saliency in IPMSM is from that of rotor reluctance. Rotor reluctance is the inductance of the rotor head magnetically coupling into the stator, that is, the mutual inductance of the stator and rotor is not zero. In IPMSM, the rotor is constructed such that the permanent magnets are buried inside a rotor head composed of electrical steel, referred to as "rotor iron". Because permanent magnets have a much lower relative permeability than that of magnetic iron, this creates a non-uniform rotor inductance that thus creates reluctance saliency in IPMSM; namely, this exhibits itself as a decreased inductance in the Direct axis relative to the Quadrature axis. SPMSM and BLDC motors do not feature rotor iron, so the inductance of the rotor head is relatively uniform. As such, these types of motors do not feature reluctance saliency [Zhao et al. 2013].

2.2.2 Saturation Saliency

The primary source of saliency in SPMSM is from that of stator saturation. Stator saturation results from rotor permanent flux coupling into the stator iron, causing the material to saturate. Figure 1 is a graph of motor flux linkage as a function of stator current which illustrates this phenomenon. The direct axis flux linkage starts at Ψ_f while the quadrature axis flux linkage starts at 0.

From figure 1 [Liu et al. 2014], this permanent excitation produces a flux through the stator in the D axis equivalent to an excitation current i_f. Since stator iron is a non-ideal magnetic material, it partially saturates at this excitation, resulting in a decrease in relative permeability and thus decrease in inductance in the D axis [Liu

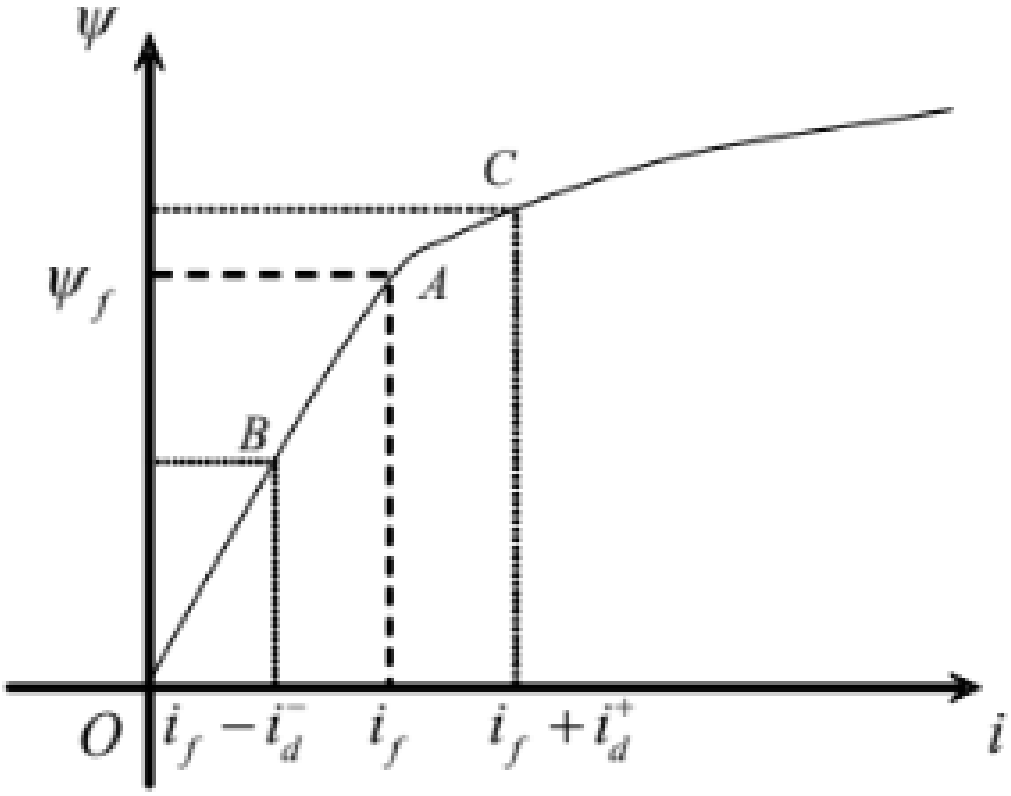

Figure 1. Rotor Flux Linkage as a function of stator current

et al. 2014]. Due to their smaller size, BLDC motors and small SPMSM often exhibit greater saturation saliency than larger motors due to the larger ratio of permanent magnet (PM) flux to stator core material.

Chapter 3

METHOD OF HIGH FREQUENCY VOLTAGE INJECTION

The following method of HF voltage injection is proposed: A high frequency pulsating voltage is injected into the estimated D axis. The resulting injected currents are used to create a position estimation error term. The position estimation error term is supplied to a PI-Type Phase-Locked Loop (PLL). PLL supplies speed and position estimates to the remainder of the FOC algorithm.

3.1 Injection Voltage Generator

Let $U_h(t)$ be the injection voltage waveform

$$U_h(t) = U_{hm} * cos(\frac{f * \pi * t}{N}) \tag{3.1}$$

Where:

- U_{hm} is the magnitude of the injected voltage
- f is the control loop frequency
- N is the frequency divider
- t is time in seconds

Note that the injection voltage has frequency equal to

$$\frac{f}{(2 * N)}$$

and angular frequency

$$\omega_h = \frac{f * \pi}{N}$$

The frequency divider can be supplied by a state machine or other source and can be varied dynamically. N is only limited by the maximum allowable magnitude of the current response that can be determined by equation 3.2. The injection voltage magnitude U_{hm} can be calculated by the equation:

$$U_{hm} = (I_{Response} * \omega_h * L_d) + V_{distortion} \tag{3.2}$$

Where:

- $I_{Response}$ is the desired magnitude of the injected current response. This can be determined based on the required current threshold to achieve a desired SNR with a given data acquisition stage
- ω_h is the angular frequency of the injection voltage, as determined by N
- L_d is the direct axis inductance
- $V_{distortion}$ is the voltage distortion incurred from inverter nonlinearities such as dead-time distortion

This voltage $U_h(t)$ is thus injected into the Estimated Direct Axis of the motor; call this vector $\hat{d}$. Figure 2 illustrates the different frames of reference when this voltage is injected. $\hat{\Theta}$ is the estimated rotor position and Θ is the true rotor position. The difference between Θ and $\hat{\Theta}$ is $\Delta\Theta$. As such $\hat{d}$ and $\hat{q}$ are the estimated synchronous direct and quadrature axes respectively. As there are multiple frames of reference, namely, stationary $\alpha - \beta$, true synchronous d-q, and estimated d-q, the Park transform is required to rotate vectors between these frames of reference. The Park transform is a rotation matrix that rotates a vector from one frame of reference to another.

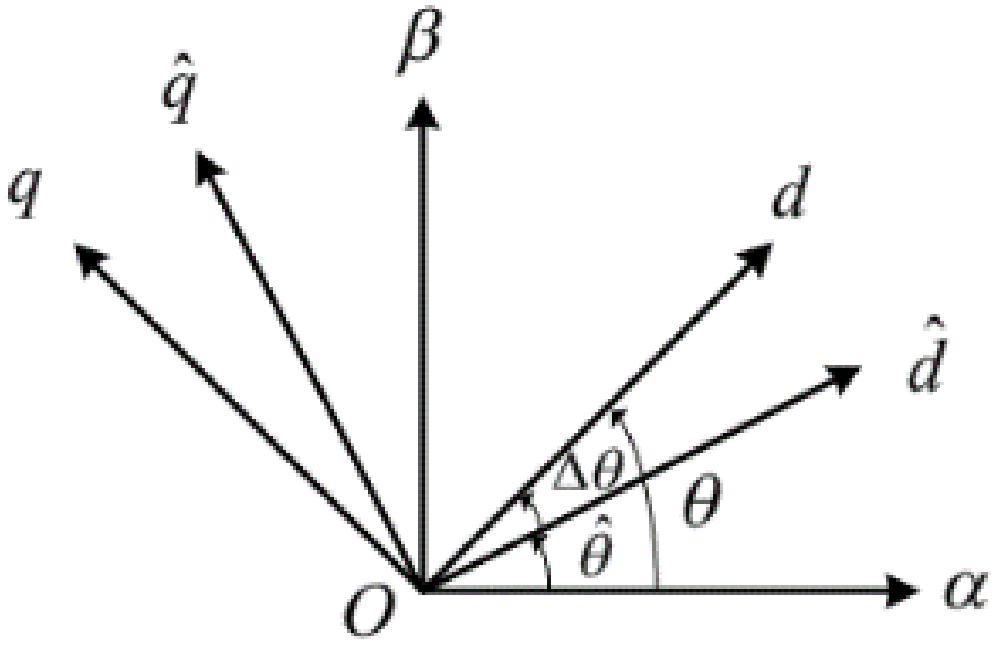

Figure 2. Diagram of Synchronous and Estimated Frames of Reference

3.2 Injection Current Response and Extraction of Error Term

As a result of the scenario depicted in figure 2 and equations 2.2 and 3.1, the injection currents are of the form [Liu et al. 2014]:

$$\begin{aligned} I_{dh} &= I_{avg} + (I_{diff} * cos(2 * \Delta\Theta)) * sin(\omega_h * t) \\ I_{qh} &= (I_{diff} * sin(2 * \Delta\Theta)) * sin(\omega_h * t) \end{aligned} \tag{3.3}$$

Where:

$$\begin{aligned} I_{avg} &= \frac{U_{hm} * (L_q + L_d)}{2 * \omega_h * L_q * L_d} \\ I_{diff} &= \frac{U_{hm} * (L_q - L_d)}{2 * \omega_h * L_q * L_d} \end{aligned} \tag{3.4}$$

These follow from equation 3.1 and the Park transform from figure 2.

Also note that $I_{avg} + I_{diff} \approx I_{Response}$.

The injection currents thus bear the position estimation error information; however, they are modulated by the frequency of the injection voltage. They can be demodulated using an envelope detector and low pass filter, resulting in equation 3.5 [Liu et al. 2014] [Zhao et al. 2013] where I_{dhm} and I_{qhm} are the envelopes of I_{dh} and I_{qh} respectively:

$$\begin{aligned} I_{dhm} &= I_{avg} + (I_{diff} * cos(2 * \Delta\Theta)) \\ I_{qhm} &= I_{diff} * sin(2 * \Delta\Theta) \end{aligned} \tag{3.5}$$

3.2.1 Error Calculation

Assuming $\Delta\Theta \approx 0$ but nonzero, When $x \approx 0$, $sin(x) \approx x$, $cos(x) \approx 1$ Dividing the quadrature axis result by the direct axis results yields:

$$\frac{I_{qhm}}{I_{dhm}} = \Delta\Theta * (1 - \frac{L_d}{L_q}) \tag{3.6}$$

Where $\frac{L_d}{L_q}$ is the reciprocal of the saliency ratio. The saliency ratio, if known, can be compensated for at this stage, otherwise, the ratio can be accommodated by the transient characteristics of the position observer whose construction is described in the next section.

3.3 Position Observer Construction

The position observer is constructed as a Phase-Locked-Loop (PLL). The PLL is constructed as a Proportional-Integral (PI) type PLL, where the error signal is multiplied by a proportional gain to obtain position, and the error signal is integrated and multiplied by an integral gain to obtain speed. The estimated speed is also used in the position estimation. Call the proportional gain Kp and the integral gain Ki.

From the transfer function of such PI-type PLLs we have $Kp = 2 * \omega$ and $Ki = \omega^2$ Where ω is the bandwidth of the PLL i.e., defines the settling time and frequency response. Rotor position and speed can be directly estimated by the outputs of this PLL [Zhang, Wang, and Xu 2017].

Chapter 4

ISSUES WITH AND PROPOSED IMPROVEMENTS TO METHOD OF HIGH FREQUENCY VOLTAGE INJECTION FOR BLDC MOTORS

4.1 Issues and Proposed Improvements

There are a number of issues that HF injection faces for use in BLDC motors. These are the need for polarity resolution of magnet poles, variable and inconsistent saliency, reduction or elimination of acoustic noise, and integration with existing state-of-the-art BEMF methods for high-speed operation. The proposed improvements in this thesis for the method of HF injection are meant to address the above issues and allow for the practical use of HF injection in BLDC motors. These improvements are 1) a hybrid frequency generator, 2) robust error calculation, 3) gain engineering of PI-type PLL, 4) observer decoupling mechanism, and 5) saliency boosting.

4.2 Identification of Magnet Polarity

One issue with the formation of the error term in equation 3.6 is that the PLL has stable points at $\Delta\Theta = 0$ and $\Delta\Theta = 180^\circ$ as a result of the $(2 * \Delta\Theta)$ term in the injected currents [Liu et al. 2014]. This term arises from the effect that saturation saliency is symmetric with magnet polarity, i.e., the direct axis inductance is equal at both the north and south poles of the rotor. This can be seen by considering the error term when $\Delta\Theta \approx 180^\circ$. Assuming $\Delta\Theta \approx 180^\circ$, Then $2 * \Delta\Theta$ is coterminal, i.e. has same vector components, with an angle $2 * \epsilon$ such that $2 * \epsilon = (2 * \Delta\Theta) - 360^\circ$. Using

the same assumptions from equation 3.6, dividing I_{qhm} by I_{dhm} in this case yields a similar form to equation 3.6:

$$\frac{I_{qhm}}{I_{dhm}} = \epsilon * (1 - \frac{L_d}{L_q}) \tag{4.1}$$

Where $\epsilon = \Delta\Theta - 180°$, indicating a stable point in the PLL at $\Delta\Theta = 180°$.
As such, there is a need to identify magnet polarity. The following polarity resolution scheme is proposed: From figure 1, the direct axis flux linkage starts at Ψ_f while the quadrature axis flux linkage starts at 0. I_f represents the equivalent excitation current required to produce the permanent magnet flux linkage in the direct axis. The slope of the line in figure 1 represents stator inductance at the given current. As can be seen from the graph in figure 1, as the flux linkage increases due to stator current, the direct axis inductance decreases significantly while the quadrature axis inductance varies only slightly. Since a pulsating voltage causes a positive and negative direct axis current, this results in harmonics in the resulting direct axis current waveform. Conceptually, this can be seen as a superimposing a term:

$$k * |sin(\omega_h * t)|$$

on the injected direct axis current waveform, where k is a scalar proportional to the change in L_d and $I_{response}$, and the sign of k dictated by the polarity of the estimated direct axis. This manifests itself as a DC component and higher order harmonics, most notably the second harmonic. The sign of k thus dictates the relative phase of the harmonics to the injection current waveform. Since the DC component will also include any system non-linearity and measurement error, the following scheme of polarity identification from [Liu et al. 2014] is proposed:

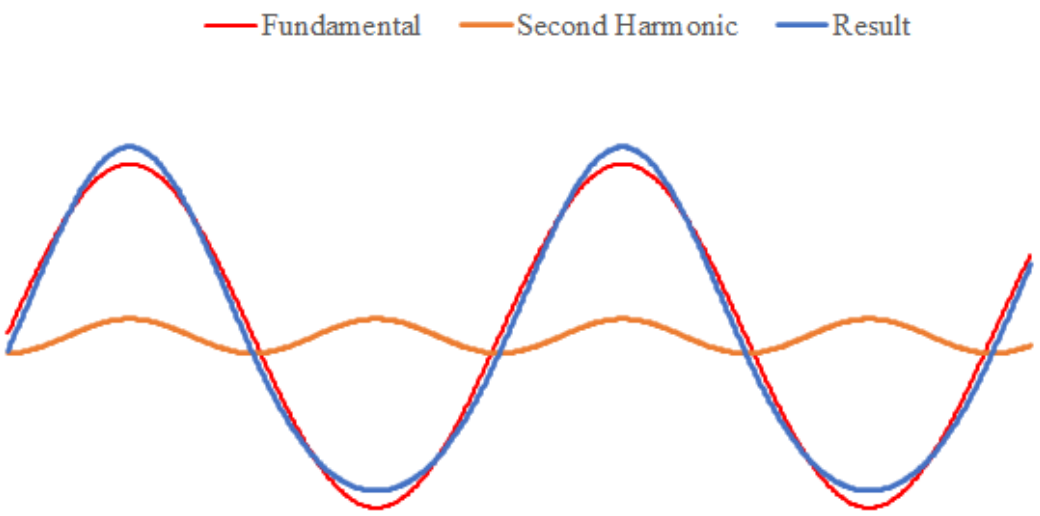

Figure 3. Resultant D axis current when polarity is correct

The second harmonic is isolated with a band-pass filter and subsequently modulated and low-pass filtered to identify its relative phase to the injection current.

Figures 3 and 4 graph of the two possible scenarios where $\Delta\Theta = 0$ and $\Delta\Theta = 180^{\circ}$ [Liu et al. 2014]. When the polarity is correct, a positive estimated direct axis voltage results in a positive real direct axis current, which results in a decrease in inductance and increase in amplitude. This is the graph depicted in figure 3. When the polarity is inverted, a positive estimated direct axis voltage results in a negative real direct axis current, which results in an increase in inductance and decrease in amplitude. This is the graph depicted in figure 4. The difference between the two is the relative phase of the second harmonic with the fundamental. The second harmonic can be isolated by a bandpass filter whose center frequency is $2 * (\frac{f}{2*N})$, where $\frac{f}{2*N}$ is the injection frequency. Since the Nyquist frequency is f / 2 where f is the control loop frequency, a

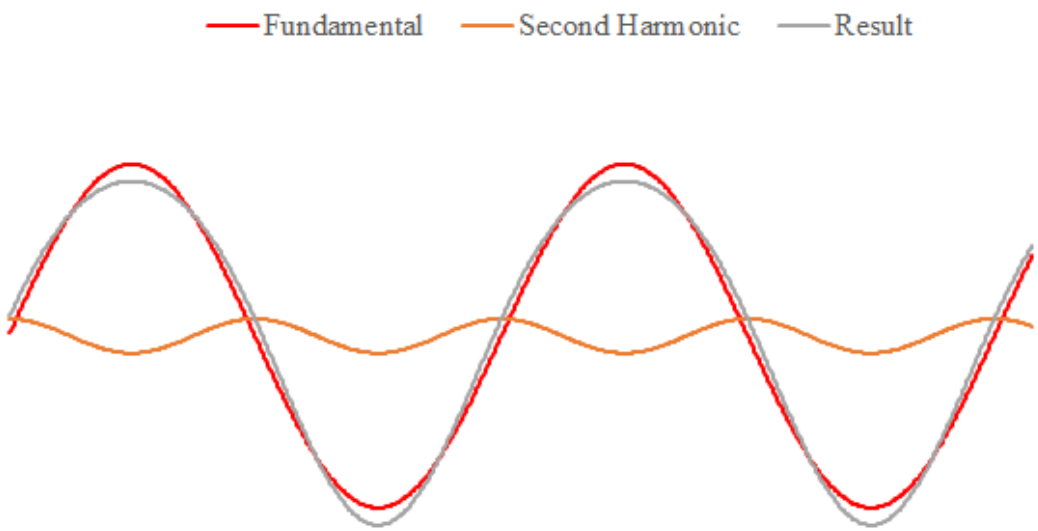

Figure 4. Resultant D axis current when polarity is inverted

divider greater than one must be used to resolve the magnet polarity. From equation 3.1, a frequency divider of N = 8 or larger is necessary. This band-pass filtered signal is then modulated with $f(t) = cos(2 * \omega_h * t)$ and subsequently low-pass filtered. In figure 4, the second harmonic has equation $p1(t) = cos(2 * \omega_h * t)$ while the the second harmonic in figure 3 has equation $p2(t) = -cos(2 * \omega_h * t)$. Thus, f(t) * p1(t) will always be positive while f(t) * p2(t) will always be negative. Subsequent low-pass filtering of these values will result in a value that is always positive or always negative. Call the result of the signal p(t). If $\Delta\Theta = 0$, then $p(t) < 0$, and when $\Delta\Theta = 180°$, then $p(t) > 0$. The polarity resolution only needs to be done once. Once the polarity has been identified, a compensation factor can be inserted into the position estimate and the frequency divider can be reduced. Once polarity resolution has completed, the computations are no longer necessary and can be bypassed by the state machine instruction.

4.3 Acoustic Noise

Especially problematic with smaller motors is that they typically have mechanical resonances in the range of the injection frequencies typically used for HF voltage injection methods (500Hz – 2kHz) [Wang, Valla, and Solsona 2020]. This often results in unacceptable amounts of acoustic noise.

4.3.1 Hybrid Frequency Injection

From equation 3.1, the frequency of the injected signal can be varied dynamically by changing the divider, N. Since polarity resolution only needs to be done once, N can be varied subsequently such that $\frac{f}{2*N}$, the injection frequency, is above the range of human perception threshold, nominally 15kHz. The proposed construction of the PLL and use of envelope detectors allows for seamless dynamic frequency scaling on-the-fly without clobbering the existing position estimate. The low-pass filter proposed for error computation smooths out disturbances from the change in frequency. Additionally, when N is set to 1, the injection voltage waveform becomes a square wave and offers increased control bandwidth. The shape of the injection waveform has minimal affect on control performance so long as it is pulsating [Zhao et al. 2013].

4.4 Variable Saliency

One issue with the proposed error calculation is that it directly embeds the saliency ratio in its value. Since BLDC motors exhibit variable saliency, this could cause certain forms of PLL and other position estimators to become unstable.

4.4.1 PLL Gain Engineering

If saliency ratio is not compensated for in the error calculation stage, then it becomes incorporated into the coefficients of the PLL such that $(1-L_d/L_q)*Kp = 2*\omega$ and $(1 - L_d/L_q) * Ki = \omega^2$. As a result, a selected range of saliency ratios can be identified such that Kp and Ki result in an overdamped system with bandwidth above a desired threshold. While the dynamic response will be degraded compared to a critically damped system, the result is that PLL will always be stable so long as the motor saliency remains above a threshold as determined by the chosen Kp and Ki.

4.5 Integration with BEMF Methods

Saliency Tracking requires that the voltage be injected in the estimated direct axis for the saliency tracking observer. This presents a problem when other observers, such as a BEMF based observer, estimate a direct axis at a different angle. If the saliency tracking estimate is not used in the Park transform, but the tracker still enabled, then the injection voltage must be rotated into the frame of the alternative estimate [Zhang, Wang, and Xu 2017]. As such, there is a need to decouple the saliency tracking observer from other position observers.

4.5.1 Observer Decoupling and Voltage Mixer

When the saliency tracking observer is activated, but the selected position estimate is not equal to the saliency tracking observer's position estimate, the synchronous voltages must be rotated so that the requested voltage is injected at the correct angle. The difference between the saliency tracking estimate and the output position estimate is Θ_{rot}. This angle is used in the Park transform to rotate the requested d axis injection voltage into the frame of the output position estimate. The result is that even though the saliency tracking observer's estimate is not used, the requested injection voltage is still injected in the frame of the saliency tracker. This allows for the use of weighted or alternative position estimates to be used in tandem with the saliency tracking observer. Weighted and alternate estimates thus allow for seamless operation between saliency tracking and BEMF position sensing methods [Zhang, Wang, and Xu 2017].

4.6 Loss of Saliency Signal

As seen from figure 1, as the quadrature axis current approaches I_f, the quadrature axis inductance approaches that of the direct axis, causing saturation saliency to disappear. Quadrature axis current must increase as torque loading increases. Loss of saliency will invariably result in large position estimation error, or even catastrophic loss of synchronization. As such, it is necessary to preserve saliency under heavy torque loading to maintain proper operation. From figure 1, injecting small amounts of D axis current can result in significant changes in the D axis inductance. As such, the following method of saliency amplification is proposed:

4.6.1 Adaptive Field Boost

As the requested quadrature axis current increases, an increasing direct axis current is also requested in proportion to the quadrature axis current, up to a limit. This requested direct axis current is added at the input of the PI current controller of the FOC algorithm. Call the maximum direct axis current that can be requested $I_{d\_inj\_max}$ and call the maximum allowable quadrature axis current I_{q_max}. By requesting this additional current, the direct axis inductance now decreases as quadrature axis inductance decreases, preserving saliency. $I_{d\_inj\_max}$ can be selected such that I_{q_max} does not exceed $I_f + I_{d\_inj\_max}$ while also maintaining reasonable torque efficiency. The field boost must only be enabled after the PLL has been given enough time to properly lock onto the rotor position.

4.7 Non-Ideal characteristics

Non-ideal characteristics present themselves as either harmonics or rotor speed coupled signals in the I_d and I_q measurements. As such, the envelope detectors and low-pass filter rejects these signals, allowing for greater PLL stability. Harmonics are rejected by the low-pass filters and speed coupled signals are rejected by the envelope detectors. As an example, non-sinusoidal BEMF is a speed coupled signal that is rejected by the envelope detector. Variable saliency due to stator reluctance i.e. concentrated windings, is a rotor speed coupled signal and is accommodated by gain engineering of the PLL. Inverter nonlinearity is a harmonic signal and is rejected by the low-pass filter.

Chapter 5

OVERALL SYSTEM

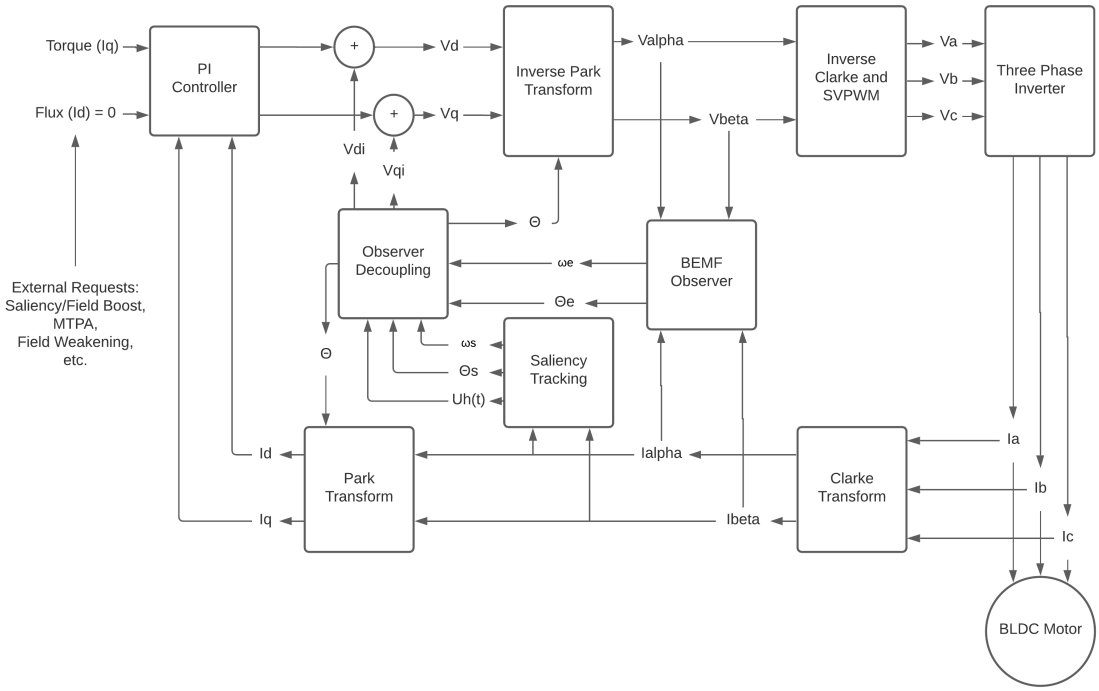

Figure 5. Overall system diagram

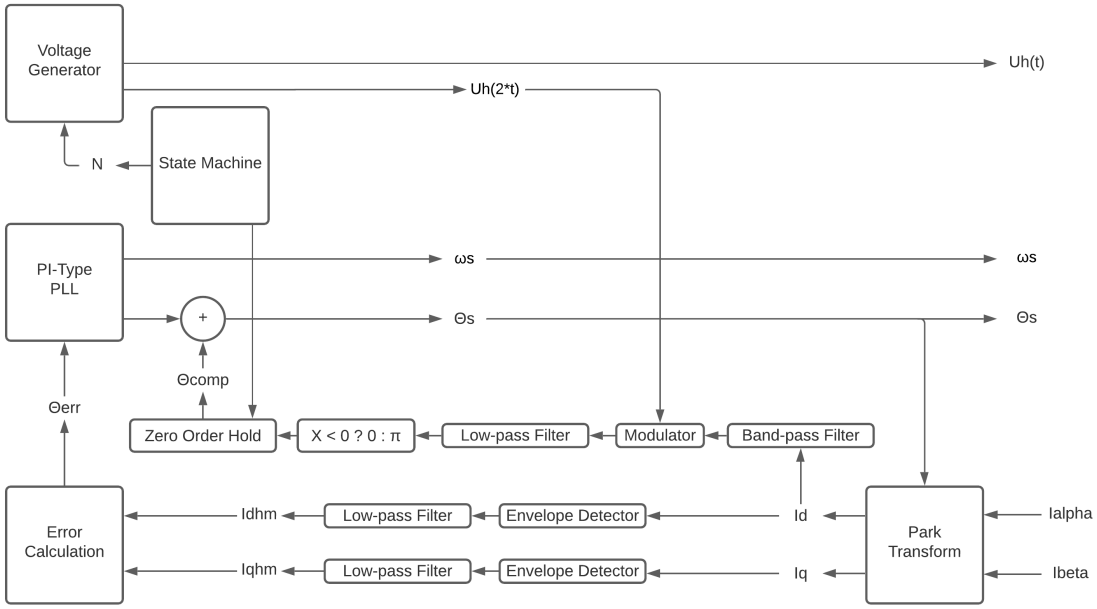

Figure 6. Saliency Tracking diagram

Figure 5 illustrates an FOC system incorporating the proposed saliency tracking algorithm. It incorporates all of the embodiements of FOC including a state-of-the-art BEMF observer. The embodiments described in this thesis are that of the Saliency Tracking block and Observer Decoupling block. The observer decoupling block decides which estimates to use and rotates any necessary injection voltages accordingly. Figure 6 illustrates the embodiments of the saliency tracking algorithm, featuring the error calculation, polarity resolution, injection voltage generator, and position and speed estimators. An exemplary state machine is included to illustrate the ability to vary the injection frequency and selectively hold the computed polarity resolution.

Chapter 6

EXPERIMENTAL RESULTS

6.1 Experimental Setup

Two experiments were performed, one to test absolute position accuracy at no load, and another to test torque efficiency at varying loads.

6.2 Position Accuracy With Encoder

The position accuracy experiment is carried out with a relatively small BLDC Motor typically found in electric scooters. The parameters of the motor are shown in table 1 below:

The accuracy of the algorithm is thus compared to a quadrature encoder mounted directly to the shaft of the motor. An image of the experimental setup is shown in figure 7. During the experiment, the motor is mechanically loaded to prevent spinning

Parameter	Value
Motor Kv	170 RPM/V
Resistance	25 milliohms
Inductance	35 uH
Pole Pairs	7
Stator Slots	12
Physical Size	63 mm x 74 mm

Table 1. Parameters of Motor used in Encoder Test

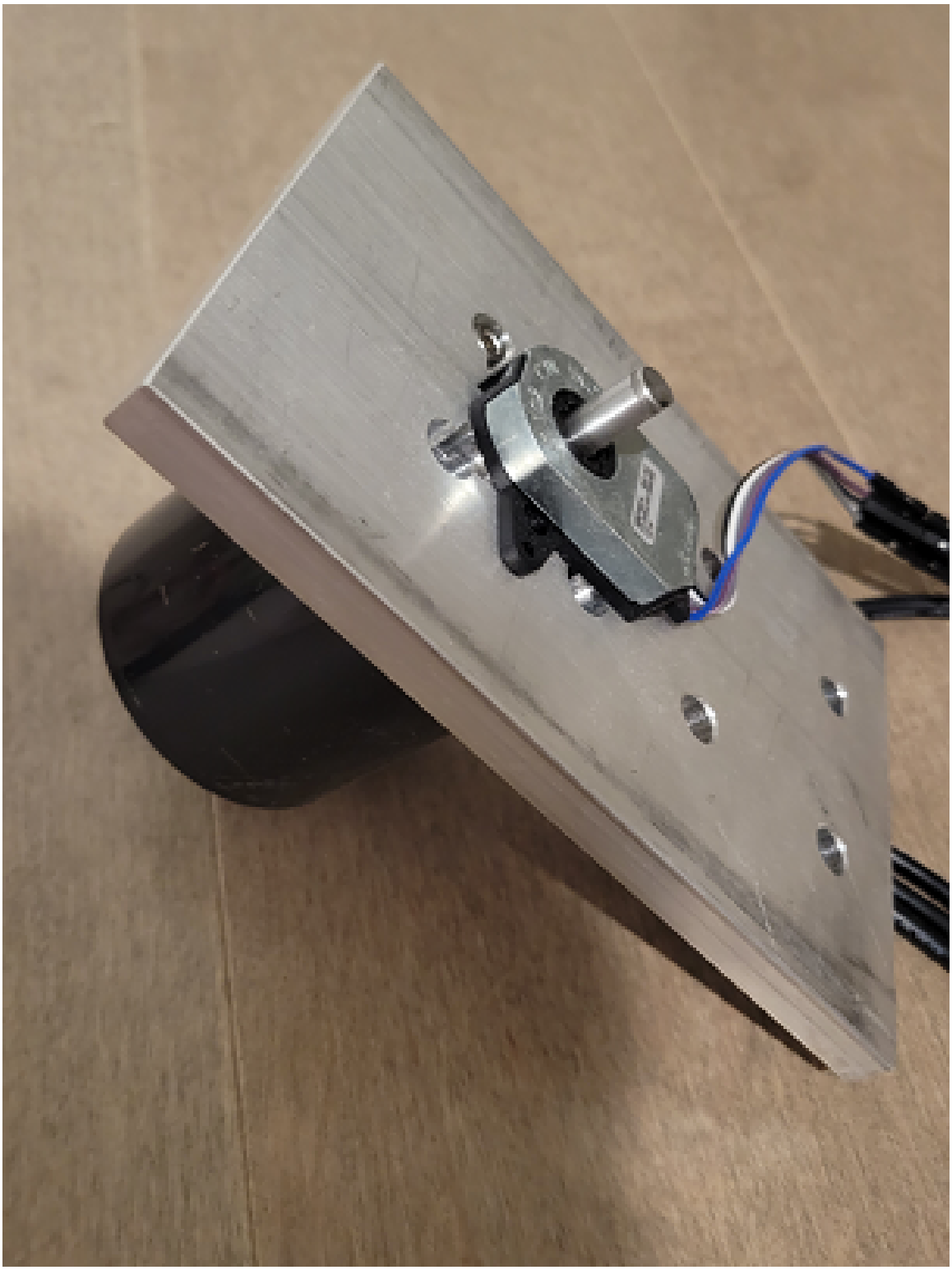

Figure 7. Image of position accuracy experiment setup

Metric	Value
Average Position Error	0.0447 rad
Maximum Position Error	0.378 rad
Equivalent Torque Efficiency	99.9%
Worst Case Torque Efficiency	92.9%

Table 2. Results of Encoder Test

while being driven at a low quadrature axis current. For brief periods, the motor is allowed to spin to up to 400RPM. The results of the experiment are illustrated in figure 8 and in table 2

6.3 Encoder Results

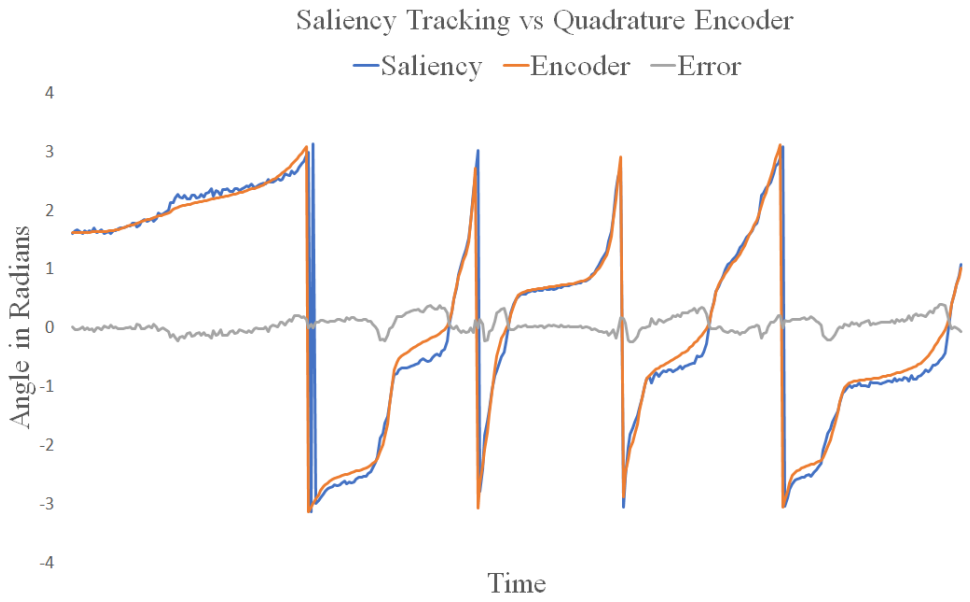

Figure 8. Results of Saliency Tracking Algorithm Compared to a Quadrature Encoder

The graph in figure 8 reveals more insight into the performance of the algorithm. In

the graph, the slope of the line indicates the rotor speed, which is this case is very low. As previously mentioned, BLDC Motors exhibit more non-ideal characteristics than their PMSM counterparts, one of which is reluctance of the stator due to relatively large gaps between stator slots; this phenomenon causes detents in the motor and is typically referred to as "cogging". Cogging exerts an opposing force on the motor and causes reductions in speed. In the graph in figure 8, the algorithm "falls into" such detents and begins lagging behind in its position estimate; these are indicated by decreases in speed. While the motor may lie between two such detents, the algorithm tracks at the center of such a detent; however, once the motor has rotated past such a detent and begun spinning, the algorithm rapidly locks onto the true rotor position and tracks very accurately as the motor's speed increases. When rotor speed drops, the algorithm once again falls into a detent; however, most BLDC Motors contain a sufficient number of stator slots to minimize these detents, and as such the worst case theoretical torque efficiency is still 93%.

6.4 Torque Efficiency

The torque efficiency experiment is carried out with a much larger motor typically used in remote control propeller aircraft. The parameters of the motor are shown in table 3 below:

This experiment is carried out on a dynamometer with an identical load motor whose windings were connected to a three-phase bridge rectifier and DC electronic load. The DC electronic load is run in constant current mode to impart a torque loading on the drive motor. The algorithm is compared to the predicted torque efficiency, torque

Parameter	Value
Motor Kv	35 RPM/V
Resistance	53.8 milliohms
Inductance	52.5 uH
Pole Pairs	20
Stator Slots	24
Physical Size	150 mm x 80 mm

Table 3. Parameters of Motor used in Torque Efficiency Test

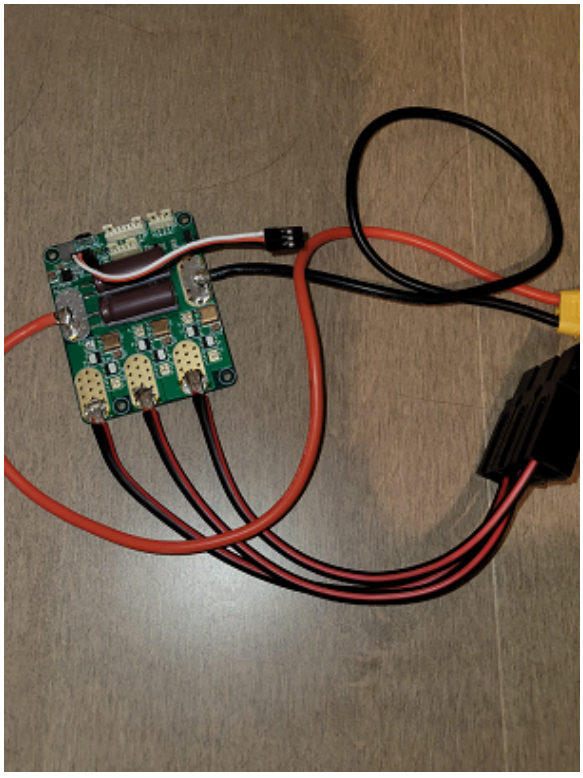

Figure 9. Image of Motor Controller hardware Used for Torque Efficiency

efficiency of a state of the art BEMF sensing method [Lee et al. 2010], and itself but with saliency boosting disabled. The algorithm ran at speeds between 0-300 RPM while the BEMF algorithm ran at a constant 400 RPM. Torque is measured using a reactionary torque sensor mounted on the load motor. The BEMF algorithm is unable to track the motor effectively below 300 RPM, and it is impossible to collect data as the motor would vibrate violently below this speed. Current is measured using real-time data streamed from hardware implementing the algorithm. An image of the controller implementing the algorithm is shown in figure 9. A graph of the results is shown in figure 10 and the Torque Per Ampere (TPA) in Newton-Meters(NM) per Ampere(A) listed in table 4. Each result has a corresponding trendline indicated by the $y = m * x$ line next to each plot where m is the slope of the trendline; the slope of the trendline is the average torque efficiency of the corresponding method i.e. saliency tracking, saliency tracking with adaptive boost, BEMF, and predicted.

6.5 Torque Efficiency Results

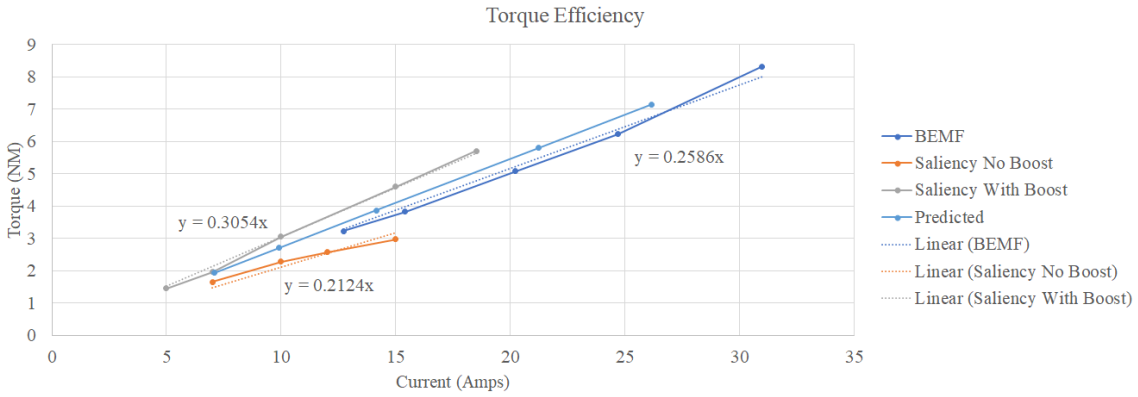

Figure 10. Results of Saliency Tracking Algorithm Compared to BEMF

Algorithm	TPA	Efficiency
Theoretical	0.273 NM/A	100%
BEMF	0.259 NM/A	95%
Saliency No Boost	0.212 NM/A	78%
Saliency With Boost	0.305 NM/A	112%

Table 4. Results of Torque Efficiency Test

As expected, a state of the art BEMF method [Lee et al. 2010] works with a reasonably high efficiency, 95%. Interesting to note is how poor the performance of the saliency tracking without field boost, only attaining about 80% of the torque that the BEMF method. This is indicative of the volatility of saliency in BLDC Motors as such a poor torque efficiency can only be the product of significant position estimation error. This indicates that under torque load, the saliency has become so weak that large amounts of error are necessary in order to extract a usable position sensing signal for the PLL. Even more interesting is that with field boosting enabled, the saliency tracking algorithm is able to achieve better than predicted torque efficiency at 112%. This is somewhat unexpected, as this implies there is a small amount of field boosting occurring; field boosting is not generally used in BLDC motors or SPMSM due to limited effectiveness. Nonetheless, this is a positive result. The result indicates that the added direct axis current is boosting the flux linkage to a small degree and that the saliency tracking algorithm is running with minimal position estimation error. The reason why a marginal field boost is possible on a motor that does not feature rotor iron is because the permanent magnet flux linkage does couple into the stator to a small degree, though not nearly as much as a specially designed IPMSM. This demonstrates that the saliency signal in such motors can be amplified advantageously. It is important to note that the direct axis current is not used in the torque efficiency calculation, only the quadrature axis current, so in reality, the

saliency tracking with field boost is still slightly less efficient than a BEMF algorithm, though it is able to operate in a speed regime where BEMF cannot. As such, this experiment demonstrates that saliency tracking can provide in the low speed and standstill operating regimes for a BLDC Motor equivalent torque performance to a BEMF algorithm that otherwise runs at high speed.

Chapter 7

CONCLUSION

In this thesis, an existing method of saliency tracking using HF pulsating frequency injection for PMSM is studied for use in BLDC Motors and small SPMSM. Due to various non-ideal characteristics, saliency tracking faces many obstacles to practical use in such motors. A number of improvements and novel modifications to the HF injection algorithm are proposed. The proposed improvements include a hybrid frequency injection voltage generator, PLL gain engineering procedure, observer decoupling method, and adaptive field boost. These allow for magnet polarity identification, reduction of acoustic noise, compatibility with wide saliency range, seamless integration with other position estimation methods, and robustness under load. As such, a practical realization of saliency tracking can be implemented for use with BLDC motors and other synchronous motors in which saliency tracking is previously not possible. Experimental results confirm the theoretical analysis.

REFERENCES

Lee, Junggi, Jinseok Hong, Kwanghee Nam, Romeo Ortega, Laurent Praly, and Alessandro Astolfi. 2010. "Sensorless Control of Surface-Mount Permanent-Magnet Synchronous Motors Based on a Nonlinear Observer." *IEEE Transactions on Power Electronics* 25 (2): 290–297. https://doi.org/10.1109/TPEL.2009.2025276.

Liu, Bing, Bo Zhou, Jiadan Wei, Haidong Liu, Jie Li, and Long Wang. 2014. "A rotor initial position estimation method for sensorless control of SPMSM." In *IECON 2014 - 40th Annual Conference of the IEEE Industrial Electronics Society,* 354–359. https://doi.org/10.1109/IECON.2014.7048524.

Wang, Gaolin, Maria Valla, and Jorge Solsona. 2020. "Position Sensorless Permanent Magnet Synchronous Machine Drives—A Review." *IEEE Transactions on Industrial Electronics* 67 (7): 5830–5842. https://doi.org/10.1109/TIE.2019.2955409.

Zhang, Guoqiang, Gaolin Wang, and Dianguo Xu. 2017. "Saliency-based position sensorless control methods for PMSM drives - A review." *Chinese Journal of Electrical Engineering* 3 (2): 14–23. https://doi.org/10.23919/CJEE.2017.8048408.

Zhao, Yue, Zhe Zhang, Cong Ma, Wei Qiao, and Liyan Qu. 2013. "Sensorless control of surface-mounted permanent-magnet synchronous machines for low-speed operation based on high-frequency square-wave voltage injection." In *2013 IEEE Industry Applications Society Annual Meeting,* 1–8. https://doi.org/10.1109/IAS.2013.6682519.

APPENDIX A

COLLECTED EXPERIMENTAL DATA

A.1 Encoder Accuracy Data

Please see attached excel document for the raw encoder data

A.2 Torque Efficiency Data

Please see attached excel document for the raw torque efficiency data